

# L2IR: Revealing Latent Intent in Graph Fraud Detection

Jinsheng Guo\*  
guojinsheng@mail.hfut.edu.cn  
Hefei University of Technology  
Hefei, China

Zhenhao Weng\*  
zhenhaoweng@mail.hfut.edu.cn  
Hefei University of Technology  
Hefei, China

Yibo Liu  
yibo.liu@mail.hfut.edu.cn  
Hefei University of Technology  
Hefei, China

Yan Qiao†  
qiaoyan@hfut.edu.cn  
Hefei University of Technology  
Hefei, China

Meng Li†  
mengli@hfut.edu.cn  
Hefei University of Technology  
Hefei, China

## Abstract

Graph fraud detection has long depended on Graph Neural Networks (GNNs) to propagate and aggregate information across relational data. A critical obstacle in practice, however, is that fraudsters frequently disguise themselves by forging numerous connections with benign users, causing fraud signals to be progressively diluted during neighborhood aggregation and undermining detection reliability. While recent efforts have used Large Language Models (LLMs) to provide rich semantic cues for fraud detection, the underlying intent behind suspicious connections remains insufficiently explored. Compounding this issue, the scarcity of annotated fraud samples makes it difficult to train detectors that remain robust under heavy camouflage. To address these gaps, we propose L2IR, an LLM-driven Latent Intent Revealing framework for graph fraud detection. By uncovering latent intent from both user behaviors and suspicious connections, L2IR extracts intent-aware representations from raw behavioral traces and reasons about the true purpose behind individual connections, effectively distinguishing supportive links from misleading ones. It further incorporates adaptive self-training to enhance robustness under limited supervision. Evaluations on two real-world datasets characterized by pervasive camouflage demonstrate that L2IR surpasses strong baselines and can function as a plug-in enhancement for a range of GNN-based detectors, improving AUPRC by up to 8.27%.

## CCS Concepts

• Computing methodologies → Artificial intelligence; • Information systems → Data mining; Social networks.

## Keywords

Fraud Detection, Graph Neural Networks, Large Language Models

## 1 Introduction

Modern online information systems, such as e-commerce platforms, review communities, social networks, and financial services, generate rich relational data among users, items, content, and transactions [2, 20, 28, 32]. Fraudulent activities in these systems reduce service quality and weaken system trust, making fraud detection an important task [17, 20]. In response, graph-based methods have become an effective paradigm. Graph-based methods model entities and interactions as graphs and exploit both node attributes

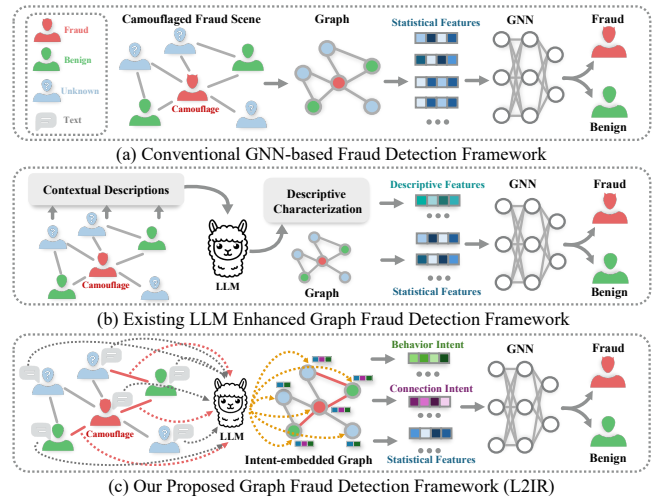


**Figure 1: Comparison of our proposed L2IR with GNN-based and LLM enhanced GNN methods under camouflage. (a) Standard GNN-based methods rely solely on graph structure. (b) LLM enhanced GNN methods incorporate dataset-level semantic descriptions to improve performance. (c) Our L2IR analyzes the intent behind each user interaction, enabling effective identification of camouflaged fraud.**

and relational structure for detection [2, 8]. Among them, Graph Neural Networks (GNNs) are widely used, since they learn center node representations by aggregating information from connected neighbors, thereby capturing patterns from neighboring nodes that are critical for distinguishing fraudulent entities from benign ones [6, 10, 26].

However, existing GNN-based fraud detection methods mainly rely on neighborhood aggregation over observed graph structures (as illustrated in Fig. 1(a) [9, 35]) and insufficiently explore fraudsters’ camouflage behaviors [4, 8]. In relation camouflage scenarios [4], fraudsters build many connections with benign users while conducting fraudulent activities on only a small fraction of them, so the benign-dominated neighborhood dilutes fraud signals during aggregation, leading to less reliable detection and increased false negatives [4, 16].

Recently, driven by the context reasoning and semantic comprehension capabilities of Large Language Models (LLMs) [7, 24, 40],

\*Equal Contribution

†Corresponding authors

existing studies leverage LLMs to incorporate rich semantics to assist graph fraud detection [9, 11, 35]. These studies have revealed potential opportunities for detecting camouflaged fraud by integrating descriptive semantic characterization with graph structural information (as illustrated in Fig. 1(b)). However, existing methods primarily restrict LLMs to generating global semantic descriptions of the dataset, without reasoning about the intent behind connections. Consequently, they fail to fully exploit the potential of LLMs for recognizing camouflaged fraud, still suffering from notable misclassifications. Even worse, real-world camouflaged fraud data is often constrained by limited supervision: the strong stealthiness of camouflaged fraud makes it extremely difficult to label such cases in datasets, leaving insufficient supervision for robust training and generalization [13, 28, 37].

To tackle these challenges, we propose **L2IR**, an LLM-driven Latent Intent Revealing framework for graph fraud detection. Specifically, L2IR leverages LLMs to analyze the behavioral semantics of each user to infer the intent behind individual connections, and then incorporates this inferred intent information into node features, thereby helping to uncover deeply camouflaged fraudulent nodes (as illustrated in Fig. 1(c)). In addition, L2IR adopts an adaptive self-training mechanism to augment supervision with reliable signals from previous stages, thereby improving robustness under limited fraud labels. Extensive experiments on two real-world datasets demonstrate the effectiveness of L2IR in fraud detection, with clear gains under camouflage and limited supervision scenarios.

In summary, our main contributions are as follows:

- We introduce a novel LLM-driven perspective for graph fraud detection under camouflage by inferring the intent behind suspicious connections with LLMs, which effectively improves the reliability of graph fraud detection.
- We propose L2IR, an intent modeling framework for graph fraud detection, which jointly models behavior intent and connection intent to extract deep semantic features. It also integrates adaptive self-training to address the scarcity of fraud labels, which enables accurate detection of heavily camouflaged fraud even under limited supervision.
- We evaluate L2IR against nine representative baselines on two real-world datasets. The results demonstrate that L2IR achieves superior empirical performance and can also serve as a plug-in to improve existing GNN-based fraud detectors.

## 2 Related Works

### 2.1 Graph Neural Networks for Fraud Detection

GNNs provide a powerful framework for capturing fraudulent patterns by aggregating neighborhood information through message propagation mechanisms [14, 15, 21, 30]. Early works directly applied classic GNNs like Graph Convolutional Networks (GCN) [10] and Graph Attention Networks (GAT) [26] to fraud detection. Subsequent works introduced various enhancements. GraphSAGE [6] introduces an inductive framework that learns to generate node embeddings by sampling and aggregating features from a node’s local neighborhood, allowing effective embedding creation for unseen nodes in dynamic or new graphs. RGTAN [33] models transaction sequences as temporal graphs and uses gated attention to capture

temporal fraud patterns. It also learns neighbor risk representations to detect multi-hop fraud structures. DiffGraph [12] employs a latent diffusion paradigm to filter noise and captures relation transitions through a bidirectional diffusion process for better node representations. To combat label scarcity, some unsupervised methods employ mutual information maximization or contrastive learning [27, 41], while SemiGNN [28] links labeled and unlabeled users via social relations and integrates heterogeneous data sources with hierarchical attention for fraud detection. However, these methods do not exploit the rich textual information and struggle to cope with the challenges posed by fraudsters deliberately camouflaging themselves as normal nodes [8, 13, 29].

### 2.2 Integrating LLMs with GNNs for Fraud Detection

In recent years, LLMs have demonstrated powerful language understanding [1, 3, 19, 25], opening a new path for graph learning by exploiting the rich textual semantics of nodes [22, 31, 39]. For instance, one paradigm utilizes GNNs to enhance LLMs, where LLMs serve as the primary predictors. GraphGPT [24] employs graph instruction tuning to translate graph structures into LLM-compatible representations, while InstructGLM [36] relies on natural language prompts for the same purpose. In both cases, the goal is to enable direct graph learning with LLMs, eliminating the need for task-specific GNN fine-tuning. DGP [11] proposes a dual granularity prompting framework retaining fine-grained text for target nodes while summarizing neighbors into coarse-grained prompts, reducing input size while preserving key fraud semantics. However, employing LLMs as the final predictor imposes significant computational resource demands and suffers from low inference efficiency. Conversely, an alternative paradigm employs LLMs to enhance GNNs, with GNNs serving as the primary predictors. TAPE [7] pioneers this by using an LLM to generate explanations as augmented node features. TouchUp-G [40] further enhances node features from pre-trained models through graph-centric finetuning to better align them with the graph structure. MLED [9] uses type-level and relation-level enhancers to integrate text knowledge with graph structure for better fraud-benign distinction. FLAG [35] employs semantic similarity sampling to filter camouflaged neighbors and leverages LLMs to extract discriminative textual features, thereby improving fraud detection, particularly on text-rich graphs. Although LLM enhanced GNNs mitigate the high cost of the LLM-as-Predictor paradigm, they fail to explicitly capture the true intent behind camouflaged connections, leaving misleading links unrecognized and contributing to elevated false negatives. Moreover, these methods still struggle under label scarcity due to limited supervision.

In contrast to prior work, L2IR leverages LLMs to infer the intent behind behaviors and connections, enhancing GNNs’ capacity to detect camouflaged fraud.

## 3 Preliminaries

We consider graph-based fraud detection on a heterogeneous graph  $\mathcal{G} = (\mathcal{V}, \mathcal{E}, \mathcal{R})$ , where  $\mathcal{V}$  is the set of  $N$  nodes,  $\mathcal{E} \subseteq \mathcal{V} \times \mathcal{V} \times \mathcal{R}$  is the set of typed edges, and  $\mathcal{R}$  is the set of relation types. Each node  $v$  is associated with a statistical feature vector  $x_v \in \mathbb{R}^d$  derived from

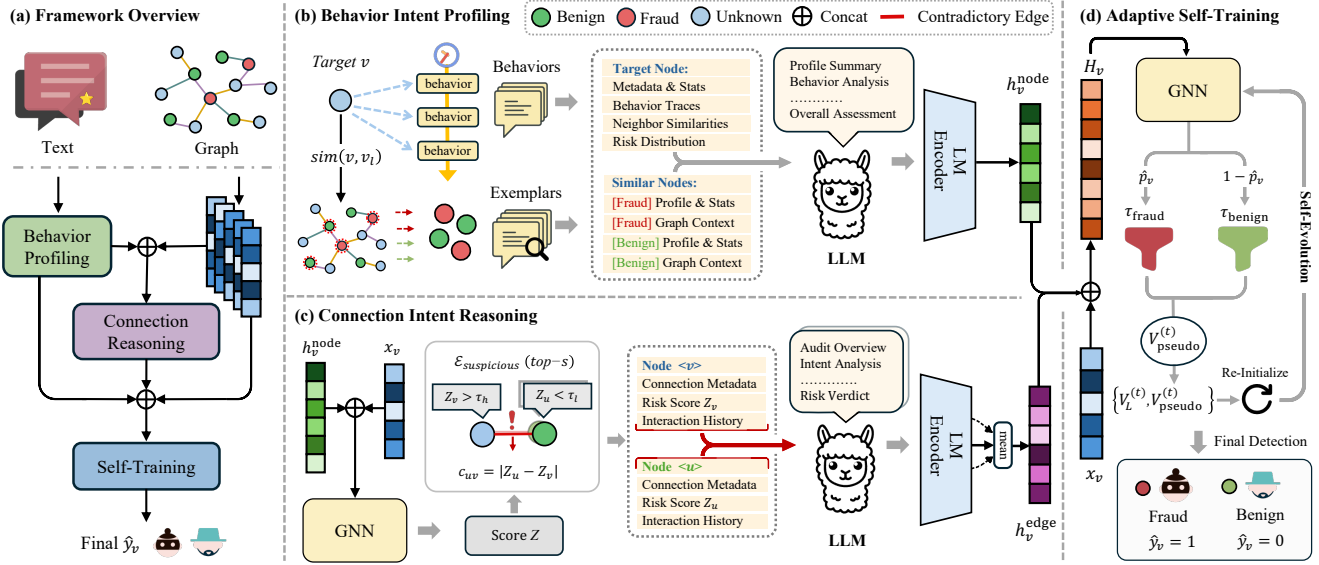


**Figure 2: The overall framework of L2IR. It consists of three key modules: (b) Behavior Intent Profiling generates intent profiles; (c) Connection Intent Reasoning infers the intent behind each connection; (d) Adaptive Self-Training progressively augments training labels to handle label scarcity.**

metadata, and a raw textual sequence  $T_v$  representing its historical behavior traces (e.g., textual reviews, item ratings, and interaction timestamps). These records are key to uncovering semantic intent hidden behind camouflaged connections. The neighborhood of node  $v$  under relation  $r$  is denoted as  $\mathcal{N}_r(v) = \{u \mid (u, v, r) \in \mathcal{E}\}$ . We further define the homogeneous projection  $\mathcal{G}_{\text{homo}} = (\mathcal{V}, \mathcal{E}_{\text{homo}})$ , where  $\mathcal{E}_{\text{homo}} = \bigcup_{r \in \mathcal{R}} \{(u, v) \mid (u, v, r) \in \mathcal{E}\}$  collapses all specific relations (e.g., reviewing the same products or giving identical ratings) into an untyped edge set to represent basic structural connectivity.

We formulate our target scenario as a graph fraud detection task operating under annotation scarcity. Formally, let  $\mathcal{V}_L \subset \mathcal{V}$  be a small set of labeled nodes with ground-truth labels  $y_v \in \{0, 1\}$  (where 1 denotes a fraudster and 0 a benign entity), and  $\mathcal{V}_U = \mathcal{V} \setminus \mathcal{V}_L$  be the remaining unlabeled nodes. In this setting, the model observes the complete topology  $\mathcal{G}$  and all node statistical features  $\mathcal{X} = \{x_v\}_{v \in \mathcal{V}}$  during training, but is supervised only by  $\mathcal{V}_L$ . Our objective is to learn a predictive function  $f_\theta : \mathcal{V} \rightarrow \{0, 1\}$  that accurately uncovers all hidden fraudsters without triggering false positives on incidentally connected benign users.

## 4 Methodology

In this section, we present the technical details of the proposed L2IR framework. It integrates LLM-driven semantic reasoning with graph structural information by modeling both node behavior intent and edge connection intent. We first outline the overall architecture, and then provide a detailed description of the constituent modules.

### 4.1 Framework Overview

At a high level, L2IR uncovers camouflaged fraudsters by aligning graph structure with intent features. As illustrated in Figure 2, L2IR consists of three key modules: **1) Behavior Intent Profiling:**

it prompts an LLM to digest raw chronological behavior traces and retrieved exemplars, and yields node-level behavior intent representations ( $h_v^{\text{node}}$ ) that complement statistical features with behavior semantic evidence. **2) Connection Intent Reasoning:** this module applies a preliminary GNN to score nodes and flag suspicious connections, then prompts an LLM to cross-audit each one, reasoning about the true intent behind the interaction. This generates edge-level connection intent representations ( $h_v^{\text{edge}}$ ) that help distinguish supportive connections from misleading ones. **3) Adaptive Self-Training:** under severe supervision scarcity, this module deploys an iterative self-training loop tailored to fraud detection. Using asymmetric confidence thresholds, it progressively adds high-confidence pseudo-labels to the training set, preventing early-round errors from cascading into later ones. Through this pipeline, semantic reasoning and structural learning reinforce each other to robustly identify camouflaged fraudsters.

### 4.2 Behavior Intent Profiling

To infer behavior intent from raw traces  $T_v$ , we prompt an LLM to analyze each target node against a group of retrieved exemplars of labeled fraud and benign nodes, allowing the model to recognize latent intent by identifying which behavioral patterns align with these exemplars.

**Dynamic Exemplar Retrieval.** To provide the LLM with references for behavior intent profiling, we dynamically retrieve a few exemplars from the labeled nodes for each target node  $v$ . Specifically, we compute the similarity between  $v$  and each labeled node  $v_l \in \mathcal{V}_L$  using a combined metric:

$$\text{sim}(v, v_l) = \alpha \cdot \text{sim}_{\text{text}}(q_v, q_{v_l}) + (1 - \alpha) \cdot \text{sim}_{\text{inter}}(I_v, I_{v_l}), \quad (1)$$

where  $q_v$  denotes the textual vector constructed from  $T_v$ ,  $I_v$  denotes the historically interacted item set of node  $v$ ,  $\text{sim}_{\text{text}}$  is the cosine

**Table 1: Core format of prompt for Behavior Intent Profiling.**


---

**[Role]** Domain-expert persona: senior fraud detection analyst specializing in review behavior and relation camouflage. The core task is to infer the target node’s behavior intent by strictly following all provided constraints and analytical requirements.

---

**[Exemplars]**  
*<k fraudulent node cases: node metadata, review statistics, rating distribution, sentiment score, graph relation context, and ground-truth label.>*  
*<k benign node cases: same format as above.>*

---

**[Target Node]**  
Node ID: <uid> Total reviews: <n> Avg. rating: <r>  
Graph Relation Context: [Neighbor Metadata | Behavior Similarities | Risk Distribution]  
Chronological Behavior Traces: [Product | Star Rating | Text Content | Helpfulness Score]

---

**[Output]** 1) Node Profile Summary → 2) Behavior Pattern Analysis → 3) Fraud Signal Analysis → 4) Overall Assessment

---

similarity between textual vectors, and  $\text{sim}_{\text{inter}}$  is the Jaccard index between item sets, where a higher value indicates a greater degree of interaction. The coefficient  $\alpha \in [0, 1]$  balances semantic content and behavioral patterns.

Based on the similarities, we construct an exemplar pool for target node  $v$ . For each class  $c \in \{0, 1\}$ , we rank nodes  $v_l \in \mathcal{V}_L^c \setminus \{v\}$  according to the similarity score  $\text{sim}(v, v_l)$ , and retrieve the top- $k$  most similar nodes to form the class-specific exemplar set  $\mathcal{S}_v^c$ . The integrated exemplar set  $\mathcal{S}_v = \mathcal{S}_v^0 \cup \mathcal{S}_v^1$  serves as a contrastive basis, which provides behaviorally grounded references for the LLM to effectively distinguish benign from fraudulent behavior intent.

**Behavior Intent Profiling with LLM.** We design a prompt to guide a pre-trained LLM, denoted by  $\mathcal{M}_{\text{LLM}}$ , in reasoning over the target node’s behavior traces  $T_v$  and the labeled exemplars  $\mathcal{S}_v$ , yielding a structured profile  $b_v = \mathcal{M}_{\text{LLM}}(\text{Prompt}_{\text{profile}}(v))$ .

As shown in Table 1, the prompt consists of four components: *Role*, *Exemplars*, *Target Node* and *Output*. The *Role* anchors the LLM in the fraud detection domain, reducing irrelevant reasoning. The *Exemplars* provides  $k$  pairs of fraud-benign cases with consistent metadata, offering contrastive behavioral references that guide the LLM toward patterns relevant to intent inference. The *Target Node* supplies the node’s statistical data, graph relation context, and chronological behavior traces, providing the LLM with concrete behavioral evidence to analyze. The *Output* enforces a structured schema progressing from profile summary to overall assessment, making the resulting profile  $b_v$  suitable for downstream encoding. The complete template for behavior intent profiling is provided in Appendix A.

**Semantic Encoding.** To integrate the captured behavior intent into node features, we encode the structured output  $b_v$  into a dense vector using a frozen pre-trained language encoder  $\mathcal{M}_{\text{Enc}}$ :

$$h_v^{\text{node}} = \mathcal{M}_{\text{Enc}}(b_v) \in \mathbb{R}^{d_s}. \quad (2)$$

The resulting embedding  $h_v^{\text{node}}$  complements the statistical features  $x_v$  as a node-level semantic prior, integrating behavior intent before

neighborhood aggregation and equipping the downstream module with richer evidence for connection intent reasoning.

### 4.3 Connection Intent Reasoning

To reason the connection intent in the graph structure, we first apply a preliminary GNN to score nodes and flag suspicious connections, then prompt an LLM to cross-audit each one by reasoning over both endpoints’ interaction histories, allowing the model to identify intent signals that distinguish supportive connections.

**Suspicious Connection Detection.** We train a preliminary GNN on the enhanced features  $[x_v || h_v^{\text{node}}]$  to produce fraud risk scores for all nodes. To enhance the robustness of scoring, we split the training set into  $K$  distinct folds and train a separate model on each fold. For labeled nodes  $\mathcal{V}_L$ , we adopt an out-of-fold (OOF) strategy. Specifically, each node falls into exactly one validation fold and is scored exclusively by that fold’s model; this prevents the bias from the remaining  $K - 1$  models that observed its label during training, thereby yielding an unbiased prediction  $\hat{p}_v^{\text{oof}}$ . For unlabeled nodes  $\mathcal{V}_U$ , since no ground-truth label is available, all  $K$  fold models provide unbiased predictions; we therefore denote by  $\hat{p}_v^{(k)}$  the prediction from the  $k$ -th fold model, and average these  $K$  predictions to improve stability. The final risk score  $Z_v$  is defined as:

$$Z_v = \begin{cases} \hat{p}_v^{\text{oof}}, & v \in \mathcal{V}_L \\ \frac{1}{K} \sum_{k=1}^K \hat{p}_v^{(k)}, & v \in \mathcal{V}_U \end{cases} \quad (3)$$

Given the node risk scores  $Z_v$ , we partition the nodes into a suspected fraud set  $\mathcal{V}_+$  and a suspected benign set  $\mathcal{V}_-$  using dual thresholds  $\tau_h$  and  $\tau_l$  ( $\tau_h > \tau_l$ ):

$$\begin{aligned} \mathcal{V}_+ &= \{v \in \mathcal{V} \mid Z_v > \tau_h\}, \\ \mathcal{V}_- &= \{v \in \mathcal{V} \mid Z_v < \tau_l\}. \end{aligned} \quad (4)$$

Based on this partition, we identify all edges from  $\mathcal{E}_{\text{homo}}$  whose two endpoints belong to different node sets—one in  $\mathcal{V}_+$  and the other in  $\mathcal{V}_-$ —and define them as the *contradictory edge set*, denoted

**Table 2: Core format of prompt for Connection Intent Reasoning.**


---

**[Role]** Senior fraud audit analyst specializing in review graphs and relation camouflage. Node  $v/u$  roles (*Suspected Fraud Node* or *Suspected Benign Node*) are dynamically assigned based on their relative preliminary risk scores  $Z$ , with the higher-scored node explicitly designated as the suspected side to analyze intent and assess evidence.

---

**[Target Connection]**  
Connection Metadata: [Node IDs & Roles | Risk scores:  $\langle Z_v \rangle / \langle Z_u \rangle$  | Contradictory Magnitude:  $\langle c_{uv} \rangle$ ]  
Chronological Interaction History ( $v$  &  $u$ ): [Product | Date | Star Rating | Text Content | Helpfulness Score]

---

**[Output]** 1) Connection Overview (risk scores, suspicious, fraud signals) → 2) Behavior Difference ( $v/u$  rating and review divergence) → 3) Connection Intent Analysis → 4) Counter Evidence and Uncertainty → 5) Risk Verdict (Low/Med/High + confidence + key evidence)

---

by  $\mathcal{E}_{\text{contra}}$ :

$$\mathcal{E}_{\text{contra}} = \mathcal{E}_{\text{homo}} \cap \left( (\mathcal{V}_+ \times \mathcal{V}_-) \cup (\mathcal{V}_- \times \mathcal{V}_+) \right). \quad (5)$$

Next, we compute the *contradictory magnitude*  $c_{uv} = |Z_u - Z_v|$  for each contradictory edge and retain the top- $s$  edges to form  $\mathcal{E}_{\text{suspicious}}$ . The budget  $s$  strictly bounds the LLM computational cost, focusing our reasoning directly on the deceptive boundaries that trigger false positives/negatives during GNN message passing.

**LLM Cross-Audit.** For each suspicious edge  $(u, v) \in \mathcal{E}_{\text{suspicious}}$ , we design a prompt incorporating the interaction histories of both endpoints alongside their risk scores  $Z_u, Z_v$  and *contradictory magnitude*  $c_{uv}$ . As shown in Table 2, the prompt consists of three components: *Role*, *Target Connection* and *Output*. The *Role* is dynamically assigned based on relative risk scores, so that the LLM can focus its reasoning on the right target. The *Target Connection* provides both the quantitative risk context and the chronological interaction histories, grounding the audit in structural evidence. The *Output* progresses from connection overview to a final risk verdict, ensuring the reasoning is systematic and the resulting report  $r_{uv}$  captures the assessed connection intent. The complete template is provided in Appendix A.

**Connection Intent Encoding.** We encode the audit report  $r_{uv}$  into a continuous representation using the language encoder  $\mathcal{M}_{\text{Enc}}$ :

$$e_{uv} = \mathcal{M}_{\text{Enc}}(r_{uv}) \in \mathbb{R}^{d_s}. \quad (6)$$

This maps the LLM’s edge-level reasoning into the GNN’s embedding space, enabling downstream aggregation to suppress deceptive message propagation.

**Feature Fusion.** To incorporate the edge-level intent embeddings  $e_{uv}$  into node-level features, we perform mean pooling over all suspicious edges connected to  $v$ :

$$h_v^{\text{edge}} = \begin{cases} \frac{1}{|\mathcal{N}_{\text{suspicious}}(v)|} \sum_{u \in \mathcal{N}_{\text{suspicious}}(v)} e_{uv}, & \text{if } \mathcal{N}_{\text{suspicious}}(v) \neq \emptyset \\ \mathbf{0}, & \text{otherwise} \end{cases} \quad (7)$$

where  $\mathcal{N}_{\text{suspicious}}(v) = \{u \mid (u, v) \in \mathcal{E}_{\text{suspicious}}\}$ . This mean pooling distills the relational intent from suspicious connections, while for nodes without suspicious edges, we set  $h_v^{\text{edge}} = \mathbf{0}$  to avoid introducing noise. Finally, we fuse the multi-view signals via concatenation:

$$H_v = [x_v \parallel h_v^{\text{node}} \parallel h_v^{\text{edge}}] \in \mathbb{R}^{d+2d_s}. \quad (8)$$

The three components  $x_v$ ,  $h_v^{\text{node}}$ , and  $h_v^{\text{edge}}$  together cover statistical features, node-level behavior intent, and edge-level connection intent, forming a comprehensive node representation.

#### 4.4 Adaptive Self-Training

To address supervision scarcity under class imbalance, we deploy a self-training loop that progressively expands the training set with high-confidence pseudo-labels. At each round  $t$ , we first re-initialize the GNN, then train it on the current labeled set  $\mathcal{V}_L^{(t)}$  with the enriched features  $H_v$ , and use it to generate pseudo-labels for the next round.

**Re-Initialization of GNN.** At the start of the  $t$ -th training round, the GNN is re-initialized from scratch. Early models trained on limited labels tend to misclassify camouflaged fraudsters as benign due to structural camouflage. If the model parameters  $\theta$  are

---

**Algorithm 1** The overall procedure of L2IR framework.

---

**Require:** Heterogeneous graph  $\mathcal{G} = (\mathcal{V}, \mathcal{E}, \mathcal{R})$ , statistical features  $X$ , textual traces  $\{T_v\}_{v \in \mathcal{V}}$ , labeled set  $\mathcal{V}_L$ , risk thresholds  $\tau_h, \tau_l$ , confidence thresholds  $\tau_{\text{fraud}}, \tau_{\text{benign}}$ , maximum self-training rounds  $T$

**Ensure:** Trained model  $f_\theta$

**Behavior Intent Profiling:**

- 1: **for** each node  $v \in \mathcal{V}$  **do**
- 2:   Retrieve exemplars  $\mathcal{S}_v$  via textual and interaction similarity
- 3:   Prompt  $\mathcal{M}_{\text{LLM}}$  with  $T_v$  and  $\mathcal{S}_v$  to generate profile  $b_v$
- 4:   Encode  $b_v$  to semantic embedding  $h_v^{\text{node}} \leftarrow \mathcal{M}_{\text{Enc}}(b_v)$

5: **end for**

**Connection Intent Reasoning:**

- 6: Train preliminary GNN on  $[x_v \parallel h_v^{\text{node}}]$  to get risk scores  $Z_v$
- 7: Partition nodes into  $\mathcal{V}_+$  and  $\mathcal{V}_-$  via thresholds  $\tau_h, \tau_l$
- 8: Retain top- $s$  contradictory edges ranked by score gap as  $\mathcal{E}_{\text{suspicious}}$
- 9: **for** each  $(u, v) \in \mathcal{E}_{\text{suspicious}}$  **do**
- 10:   Cross-audit  $(u, v)$  via  $\mathcal{M}_{\text{LLM}}$  to generate audit report  $r_{uv}$
- 11:   Encode audit to relational embedding  $e_{uv} \leftarrow \mathcal{M}_{\text{Enc}}(r_{uv})$

12: **end for**

- 13: Mean-pool  $\{e_{uv}\}$  to obtain edge representation  $h_v^{\text{edge}}$
- 14: Concatenate the features:  $H_v \leftarrow [x_v \parallel h_v^{\text{node}} \parallel h_v^{\text{edge}}]$

**Adaptive Self-Training:**

- 15: Initialize labeled set  $\mathcal{V}_L^{(0)} \leftarrow \mathcal{V}_L$
  - 16: **for**  $t = 0, 1, \dots, T - 1$  **do**
  - 17:   Re-initialize parameters  $\theta$  from scratch
  - 18:   Update  $f_\theta$  by training on  $H_v$  with  $\mathcal{V}_L^{(t)}$
  - 19:   Generate pseudo-labels  $\hat{\mathcal{V}}_1, \hat{\mathcal{V}}_0$  via thresholds  $\tau_{\text{fraud}}, \tau_{\text{benign}}$
  - 20:    $\mathcal{V}_L^{(t+1)} \leftarrow \mathcal{V}_L^{(t)} \cup \hat{\mathcal{V}}_1 \cup \hat{\mathcal{V}}_0$
  - 21: **end for**
  - 22: **return** Trained model  $f_\theta$
- 

carried over iteratively, these biases can propagate through multi-hop message passing and compound across rounds. Re-initializing at each round forces the model to relearn from the updated labeled set, allowing it to progressively correct earlier misclassifications as more reliable pseudo-labels are incorporated.

**GNN Training.** With freshly initialized parameters, the GNN is trained on  $\mathcal{G}_{\text{homo}}$  using the enriched features  $H_v$  and the current labeled set  $\mathcal{V}_L^{(t)}$ . The model minimizes the binary cross-entropy loss:

$$\mathcal{L} = -\frac{1}{|\mathcal{V}_L^{(t)}|} \sum_{v \in \mathcal{V}_L^{(t)}} [y_v \log \hat{p}_v + (1 - y_v) \log(1 - \hat{p}_v)], \quad (9)$$

where  $\hat{p}_v$  is the fraud probability for node  $v$  predicted by the current model. Once training converges, the model produces  $\hat{p}_v$  for all nodes in  $\mathcal{V}_U$  for pseudo-label generation.

**Pseudo-Label Generation.** Since  $\hat{p}_v$  represents the model’s confidence that node  $v$  is fraudulent,  $1 - \hat{p}_v$  naturally serves as the confidence for the benign class. Accordingly, we identify a pseudo-fraud set  $\hat{\mathcal{V}}_1$  and a pseudo-benign set  $\hat{\mathcal{V}}_0$  from the unlabeled nodes

**Table 3: Statistics of the evaluation datasets.**

	#Nodes	#Fraud (%Ratio)	Relation	#Edges	Avg. Behav. Sim.	Avg. Conn. Sim.
Amazon	11,944	821 (6.87%)	U-P-U	177,547	0.71	16.72%
			U-S-U	545,838	0.71	5.09%
			U-V-U	3,036,733	0.70	6.35%
			ALL	3,515,011	0.70	7.93%
Yelp	12,024	1,442 (11.99%)	U-P-U	877,840	0.78	9.80%
			U-S-U	2,268,662	0.76	6.71%
			U-V-U	1,174,921	0.74	15.45%
			U-T-U	1,225,192	0.78	7.00%
			ALL	4,797,417	0.76	9.60%

$\mathcal{V}_U$  by applying asymmetric confidence thresholds ( $\tau_{\text{benign}} > \tau_{\text{fraud}}$ ):

$$\begin{aligned}\hat{\mathcal{V}}_1 &= \{v \in \mathcal{V}_U \mid \hat{p}_v \geq \tau_{\text{fraud}}\}, \\ \hat{\mathcal{V}}_0 &= \{v \in \mathcal{V}_U \mid 1 - \hat{p}_v \geq \tau_{\text{benign}}\}.\end{aligned}\quad (10)$$

This design helps mitigate the inherent class imbalance:  $\tau_{\text{benign}}$  is set higher to reduce the risk of majority-class dominance, while  $\tau_{\text{fraud}}$  is kept relatively relaxed to maintain sufficient coverage of the minority fraud class. Using these confident subsets, we expand the labeled set for the next round:

$$\mathcal{V}_{\text{pseudo}}^{(t)} = \hat{\mathcal{V}}_1 \cup \hat{\mathcal{V}}_0, \quad \mathcal{V}_L^{(t+1)} = \mathcal{V}_L^{(t)} \cup \mathcal{V}_{\text{pseudo}}^{(t)}.\quad (11)$$

This iterative expansion progressively extends supervision coverage to more covert fraudsters across rounds, and is capped by the maximum number of self-training rounds.

Algorithm 1 summarizes the complete procedure of L2IR. The first stage (Lines 1–5) performs *Behavior Intent Profiling* for all nodes. The second stage (Lines 6–14) conducts *Connection Intent Reasoning* to identify and audit contradictory edges, producing the enriched features  $H_v$ . The third stage (Lines 15–21) runs the *Adaptive Self-Training* loop. The final line returns the trained model, which can be used to detect camouflaged fraudulent nodes.

## 4.5 Scalability Analysis

To ensure high scalability, L2IR decouples heavy LLM inference from iterative GNN training. LLM profiling and reasoning require  $O(|\mathcal{V}| + |\mathcal{E}_{\text{suspicious}}|)$  forward passes, executed offline as one-time preprocessing. Selecting suspicious connections by node scores ( $|\mathcal{E}_{\text{suspicious}}| \ll |\mathcal{E}_{\text{homo}}|$ ) avoids exhaustive evaluation over all edges. The self-training trains the GNN with  $O(T \cdot |\mathcal{E}_{\text{homo}}| \cdot L \cdot d_h)$  complexity, where  $L$  is the layer count and  $d_h$  the hidden dimension. With rapid convergence ( $T \leq 10$ ) and negligible feature fusion overhead, L2IR’s computational cost remains comparable to standard GNN baselines, ensuring efficient scaling to large real-world graphs.

## 5 Experiments

In this subsection, we evaluate L2IR’s performance in two ways: (i) combining L2IR with CARE-GNN [4] as a standalone model, and (ii) applying L2IR as a plug-in to multiple GNN-based graph fraud detection models.

## 5.1 Experimental Setup

**Datasets.** We evaluate L2IR on two real-world datasets, Amazon [18] and Yelp [20], which are widely used benchmarks for graph fraud detection. In both datasets, each node represents a user associated with statistical features derived from review metadata. Table 3 summarizes the statistics of the two datasets.

Specifically, the Amazon dataset comprises musical instrument reviews, structured into a graph where nodes represent users with 25-dimensional feature vectors. It contains three relation types [4]: users reviewing at least one same product (U-P-U); users posting reviews with the same star rating within one week (U-S-U); and users with top-5% mutual review text similarity (as measured by TF-IDF) (U-V-U). The Yelp dataset [20] consists of restaurant reviews from New York City, featuring 32-dimensional node attributes. Following similar relation construction strategies [4], it contains four relation types: users reviewing the same product within a sliding window of  $K=10$  reviews (U-P-U); users assigning an identical extreme star rating within the same calendar month (U-S-U); users sharing top- $k$  ( $k=100$ ) text similarity across all review texts (U-V-U); and users whose posting activity concentrates on the exact same calendar day regardless of the products reviewed, with co-occurrence capped at 50 (U-T-U).

Avg. Behav. Sim. and Avg. Conn. Sim. in Table 3 reflect the camouflage degree of fraudulent nodes in the datasets, which will be elaborated in Section 5.2.

**Evaluation Metrics.** To comprehensively evaluate model performance, we employ three widely adopted metrics: AUROC, AUPRC and MacroF1. AUROC captures the model’s ability to rank positive instances above negative ones across all possible thresholds, reflecting the overall separability between classes. MacroF1 averages the F1 scores of both positive and negative classes, providing a balanced evaluation that treats both classes equally regardless of class distribution. AUPRC focuses on performance on the positive class by balancing precision and recall, making it more sensitive to improvements on rare classes.

**Baselines.** We compare L2IR with nine state-of-the-art baselines for graph fraud detection, including GraphSAGE [6], FdGars [29], Player2Vec [38], CARE-GNN [4], GraphConsis [16], BWGNN [23], PMP [42], DiffGraph [12], and RGTAN [33]. We reproduce all baselines using the publicly released codebases provided by the respective authors.

**Implementation.** For a fair comparison, each baseline is configured according to the hyperparameter settings recommended in its original paper, and all methods are optimized with Adam. Besides, we set the training batch size to 128 on Amazon and 256 on Yelp. The confidence thresholds are set as  $\tau_{\text{fraud}} = 0.90$  and  $\tau_{\text{benign}} = 0.95$  on Amazon, and  $\tau_{\text{fraud}} = 0.80$  and  $\tau_{\text{benign}} = 0.85$  on Yelp. The maximum number of self-training rounds is set to 3 on Amazon and 2 on Yelp. For behavior intent profiling, we set the number of retrieved exemplars per class to  $k = 2$ . For connection intent reasoning, we set  $\tau_h = 0.80$ ,  $\tau_l = 0.20$ , and  $s = 4000$  to retain suspicious connections ranked by contradictory magnitude while bounding the LLM inference cost. Each method undergoes ten trials with different random seeds, and we report the mean and standard deviation. For the LLM components in L2IR, we use *Llama-3.1-8B* [5] as the default backbone, and additionally evaluate *Qwen3-8B* [34] when

**Table 4: Performance of L2IR as a standalone model under various training ratios (AUROC, MacroF1, and AUPRC in percentage). Bold: best, Underline: second best.**

Dataset	Metric	Train%	Graph-SAGE	FdGars	Player-2Vec	CARE-GNN	Graph-Consis	BWGNN	PMP	Diff-Graph	RGTAN	L2IR
Amazon	AUROC	40%	75.24±1.12	78.89±0.94	81.24±1.65	95.76±0.31	96.15±0.45	96.44±1.63	<b>97.78±0.12</b>	97.41±0.21	96.01±1.22	97.62±0.28
		30%	74.86±0.94	78.49±0.64	81.51±1.68	95.40±0.44	94.42±1.14	94.97±3.16	<b>97.70±0.11</b>	96.97±0.12	94.61±2.17	97.58±0.24
		20%	74.92±0.90	78.74±0.53	82.03±1.67	95.31±0.50	94.03±0.62	94.38±2.00	<u>97.44±0.42</u>	96.71±0.51	93.38±2.36	<b>97.53±0.27</b>
		10%	74.58±0.73	78.47±0.39	81.71±1.63	94.97±0.48	93.84±0.56	93.29±3.08	<u>96.70±0.46</u>	96.03±0.48	93.40±0.93	<b>97.10±0.31</b>
	MacroF1	40%	54.93±2.70	64.96±0.57	68.21±1.80	88.84±0.40	90.71±0.34	91.51±0.56	91.80±0.56	90.40±0.97	<u>91.87±0.42</u>	<b>92.46±0.66</b>
		30%	57.45±2.04	64.54±0.51	68.42±1.85	88.18±0.65	90.48±0.21	91.57±0.40	<b>91.84±0.41</b>	90.36±0.74	91.23±0.77	91.74±0.53
		20%	56.27±2.64	64.91±0.28	69.02±1.80	88.54±0.72	90.97±0.18	91.19±0.68	91.18±0.35	90.20±0.67	<u>91.31±0.66</u>	<b>91.68±0.78</b>
		10%	54.88±1.95	64.60±0.62	68.71±2.21	88.27±1.05	<u>90.53±0.25</u>	90.33±0.41	90.30±0.50	88.71±1.22	89.56±0.59	<b>91.43±1.24</b>
	AUPRC	40%	20.67±1.58	26.84±0.98	40.25±2.64	85.01±0.65	84.48±0.82	84.65±2.81	<u>88.74±0.85</u>	86.95±0.95	87.70±2.10	<b>89.05±0.61</b>
		30%	20.40±1.08	26.41±0.69	41.05±2.97	84.28±0.82	79.18±5.63	82.23±3.51	<u>87.53±0.40</u>	86.24±0.78	84.86±2.51	<b>87.81±0.78</b>
		20%	19.81±1.17	26.74±0.31	41.71±2.86	84.67±0.95	82.36±0.52	81.87±2.67	<u>86.67±0.38</u>	86.01±0.63	84.66±2.53	<b>87.90±0.84</b>
		10%	19.45±0.37	26.60±0.72	41.04±3.91	83.87±0.70	81.78±0.58	81.30±2.90	<u>86.18±0.37</u>	84.19±1.06	84.03±1.91	<b>87.52±0.73</b>
Yelp	AUROC	40%	60.82±1.38	72.80±0.44	65.23±1.51	88.62±0.36	87.02±0.39	88.26±0.70	<b>92.90±0.25</b>	88.11±0.25	89.35±0.86	91.85±0.48
		30%	61.57±1.56	73.12±0.17	65.23±1.91	87.95±0.69	86.21±0.35	88.69±0.49	<u>91.38±0.20</u>	87.48±0.41	88.02±0.68	<b>91.72±0.62</b>
		20%	61.02±1.34	73.21±0.25	63.67±2.81	87.40±0.62	84.89±2.18	87.56±1.09	<u>88.50±0.31</u>	86.92±0.71	86.97±0.88	<b>90.42±0.77</b>
		10%	60.02±1.61	73.03±0.34	61.08±9.32	<u>86.33±0.45</u>	81.64±3.21	85.87±0.54	86.00±0.17	85.94±0.76	86.05±0.59	<b>89.23±0.49</b>
	MacroF1	40%	48.47±2.17	60.49±0.41	59.52±1.32	73.78±1.95	75.97±0.01	78.27±0.62	<b>78.92±0.66</b>	76.25±0.66	<u>78.41±1.10</u>	78.15±1.62
		30%	49.60±1.90	60.68±0.31	59.57±1.74	72.99±0.21	74.56±0.32	<b>78.39±0.85</b>	77.89±0.17	75.89±0.78	<u>77.96±0.65</u>	<u>78.02±0.54</u>
		20%	49.38±2.25	60.74±0.34	58.23±2.59	71.94±1.07	74.17±1.89	75.57±0.59	74.83±0.38	74.99±0.94	<u>75.88±1.06</u>	<b>77.45±1.56</b>
		10%	49.72±2.69	60.72±0.28	57.40±4.07	70.93±1.75	71.51±2.68	74.11±1.42	72.10±0.37	73.21±1.20	<u>74.67±1.18</u>	<b>75.17±1.48</b>
	AUPRC	40%	19.37±1.45	24.45±0.68	24.04±2.77	64.81±0.96	57.93±0.88	66.58±1.18	<b>71.01±0.98</b>	62.70±0.86	68.87±1.74	69.86±0.89
		30%	19.82±1.41	24.72±0.19	24.57±2.81	62.31±1.07	52.78±1.66	67.19±2.51	<u>67.58±0.69</u>	62.32±1.62	66.36±1.62	<b>68.51±1.19</b>
		20%	18.98±1.29	24.99±0.39	22.28±4.40	60.57±1.37	50.59±6.24	64.23±1.54	<u>60.29±1.19</u>	60.00±1.80	<u>64.39±1.36</u>	<b>65.44±1.06</b>
		10%	18.79±1.41	24.90±0.55	21.44±5.82	57.74±1.98	43.15±9.99	58.74±2.18	53.93±0.25	56.87±1.87	<u>58.82±1.75</u>	<b>60.93±2.03</b>

L2IR is applied as a plug-in to multiple GNN-based methods. All experiments are executed on NVIDIA RTX 3090 24GB GPU.

## 5.2 Fraudster Camouflage Analysis

To verify the degree of fraudster camouflage in our evaluation datasets, we employ two complementary metrics introduced in [16]. The first is *behavior similarity* (abbreviated as Behav. Sim.), which ranges from 0 to 1 and quantifies the extent to which a fraudulent node’s behavior profile resembles those of its neighbors. It is computed as the average pairwise Gaussian kernel (RBF) similarity between the feature vector of a fraudulent node and those of its connected neighbors. A value closer to 1 indicates stronger behavioral resemblance, making fraudulent nodes more difficult to distinguish from benign ones. The second is *connection similarity* (abbreviated as Conn. Sim.), defined as the fraction of a fraudulent node’s neighbors that are also fraudulent. It directly reflects the degree to which fraudsters embed themselves within benign neighborhoods: a lower value indicates deeper camouflage, as the fraudulent node is surrounded predominantly by benign neighbors. Table 3 reports both metrics across all relation types on the two datasets. From the table, the behavior similarity scores of both datasets are consistently high, maintaining an average of 0.70 or higher across all relations. Connection similarity scores are consistently low, with

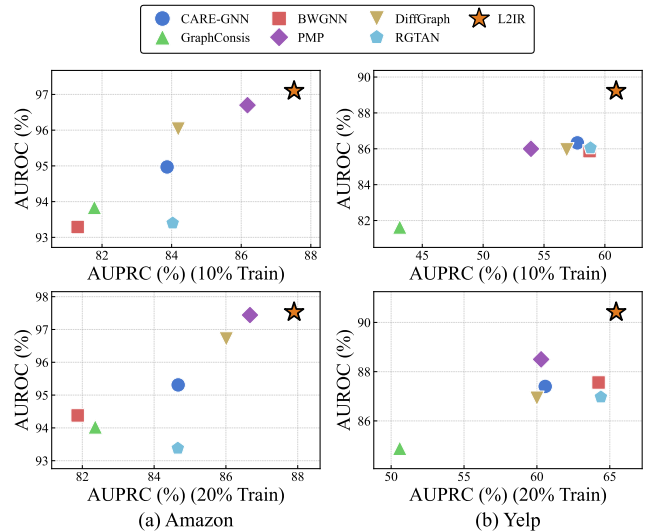


**Figure 3: AUROC vs. AUPRC at 10% and 20% training ratios. Each point represents a method; the upper-right corner indicates better joint performance.**

**Table 5: Performance of L2IR as a plug-in module to GNN-based methods under the 50% labeled setting with a fixed 40% train ratio (AUROC and AUPRC in percentage).**

Methods	Amazon		Yelp	
	AUROC	AUPRC	AUROC	AUPRC
GraphSAGE	73.99±1.42	25.23±1.07	61.10±1.32	19.84±0.86
+L2IR <sub>Qwen3-8B</sub>	75.05±0.73	26.12±0.97	63.84±1.28	21.61±1.82
+L2IR <sub>Llama-3.1-8B</sub>	75.19±1.68	26.24±1.43	63.78±1.35	21.03±1.71
FdGars	80.73±0.72	32.61±0.92	74.40±1.24	26.02±1.81
+L2IR <sub>Qwen3-8B</sub>	81.68±0.49	33.34±0.76	75.62±1.13	26.63±1.54
+L2IR <sub>Llama-3.1-8B</sub>	81.52±0.53	33.45±0.82	75.81±1.09	26.80±1.62
Player2Vec	82.92±1.23	46.51±2.55	66.32±0.61	26.90±1.92
+L2IR <sub>Qwen3-8B</sub>	85.85±0.64	49.98±1.71	68.97±1.02	29.96±1.01
+L2IR <sub>Llama-3.1-8B</sub>	85.93±0.71	48.81±0.83	69.14±1.43	30.11±0.89
GraphConsis	92.46±0.31	80.51±0.66	84.03±3.51	49.48±6.02
+L2IR <sub>Qwen3-8B</sub>	94.33±1.16	84.37±0.85	84.96±1.10	51.72±4.65
+L2IR <sub>Llama-3.1-8B</sub>	94.21±1.24	84.19±0.42	85.12±1.18	51.07±3.43
CARE-GNN	90.60±0.56	79.63±1.06	83.11±0.74	58.22±2.35
+L2IR <sub>Qwen3-8B</sub>	94.19±0.74	84.36±0.98	87.70±0.67	65.01±1.61
+L2IR <sub>Llama-3.1-8B</sub>	93.82±0.81	84.93±0.89	88.04±0.91	64.82±1.87
BWGNN	86.81±0.67	84.99±0.70	84.85±0.26	54.43±3.53
+L2IR <sub>Qwen3-8B</sub>	96.73±0.39	85.96±0.83	87.47±1.75	68.02±3.13
+L2IR <sub>Llama-3.1-8B</sub>	96.59±0.47	85.21±0.95	86.32±1.58	66.96±2.84
PMP	88.01±0.37	86.56±0.30	90.76±0.24	73.12±1.19
+L2IR <sub>Qwen3-8B</sub>	94.72±0.46	88.20±1.17	91.64±0.49	78.76±0.92
+L2IR <sub>Llama-3.1-8B</sub>	95.20±0.79	87.64±0.55	91.07±0.36	78.25±0.61
DiffGraph	96.20±0.39	83.39±2.08	85.98±0.70	56.09±3.24
+L2IR <sub>Qwen3-8B</sub>	97.05±0.25	88.22±0.62	87.68±0.84	63.98±2.50
+L2IR <sub>Llama-3.1-8B</sub>	96.91±0.28	88.14±0.57	87.77±0.41	63.01±2.18
RGTAN	93.65±2.27	82.48±3.58	84.33±2.86	65.45±3.45
+L2IR <sub>Qwen3-8B</sub>	94.51±1.74	84.53±2.17	89.02±2.16	73.72±2.39
+L2IR <sub>Llama-3.1-8B</sub>	94.28±1.63	84.66±2.08	88.91±2.21	73.14±2.53

the majority of each fraudulent node’s connections leading to benign neighbors. On Yelp, for instance, only 6.71% and 7.00% of the neighbors of fraudulent nodes under U-S-U and U-T-U relations are also fraudsters. These results demonstrate our evaluation datasets exhibit a high degree of camouflaged fraud.

### 5.3 Overall Performance

**L2IR as a Standalone Model.** Table 4 presents the accuracy comparison between L2IR combined with CARE-GNN [4] as a standalone model and the baseline methods. We adopt CARE-GNN as the fixed backbone due to its high computational efficiency. All experiments are conducted on fully annotated datasets under training ratios ranging from 10% to 40%, with the remaining nodes used as the test set.

As shown in Table 4, L2IR achieves the best or second-best results under most scenarios, and the advantage tends to become more pronounced as the training ratio decreases. Notably, with only 20% and 10% training data, L2IR outperforms all baselines across all metrics and consistently achieves the best results on both datasets.

**Table 6: Ablation study results under 50% labeled setting with a fixed 40% train ratio (AUROC and AUPRC in percentage).**

Methods	Variant			Amazon		Yelp	
	BI	CI	ST	AUROC	AUPRC	AUROC	AUPRC
BWGNN	✓	✓	✓	96.73±0.39	85.96±0.83	87.47±1.75	68.02±3.13
		✓	✓	93.84±0.57	85.62±0.85	86.54±1.40	63.29±1.17
	✓		✓	90.37±0.98	85.14±1.25	85.77±1.85	60.19±2.27
	✓	✓		92.89±0.48	85.47±2.19	86.21±1.36	64.81±0.99
PMP	✓	✓	✓	94.72±0.46	88.20±1.17	91.64±0.49	78.76±0.92
		✓	✓	93.28±0.90	87.23±0.73	91.22±0.51	76.87±0.73
	✓		✓	91.35±0.61	86.91±1.04	91.07±0.74	75.05±0.97
	✓	✓		92.85±0.54	87.52±0.87	91.51±0.62	76.50±0.79
DiffGraph	✓	✓	✓	97.05±0.25	88.22±0.62	87.68±0.84	63.98±2.50
		✓	✓	96.88±0.37	86.86±0.90	87.10±0.85	61.81±2.09
	✓		✓	96.43±0.63	85.13±0.75	86.21±1.04	59.48±2.36
	✓	✓		96.71±0.42	86.69±1.16	86.72±0.96	62.04±2.14
RGTAN	✓	✓	✓	94.51±1.74	84.53±2.17	89.02±2.16	73.72±2.39
		✓	✓	94.33±1.24	84.01±2.01	87.35±1.01	70.66±1.65
	✓		✓	93.94±1.78	82.82±2.14	86.84±2.17	68.47±2.37
	✓	✓		94.37±1.39	83.69±1.46	87.79±2.32	71.37±2.49

Specifically, on Amazon, L2IR achieves the best AUPRC at both 20% and 10% training ratios, surpassing the best baseline (PMP) by relative margins of 1.42% and 1.55%, respectively. On Yelp, at 20% training ratio, L2IR improves AUROC by 2.17% over PMP and AUPRC by 1.63% over RGTAN; at 10%, the relative gains further increase to 3.36% in AUROC over CARE-GNN and 3.59% in AUPRC over RGTAN. For MacroF1, L2IR achieves improvements of 2.07% over RGTAN on Yelp (20%) and 0.99% over GraphConsis on Amazon (10%). As further illustrated in Figure 3, comparing AUROC against AUPRC at these low training ratios shows that L2IR consistently occupies the optimal upper-right region. These results confirm that by inferring connection intent to expose camouflaged fraud, L2IR improves detecting camouflaged fraudsters while maintaining stable fraud-benign discrimination, and becomes especially effective under limited supervision.

**L2IR as a Plug-in for GNNs.** Table 5 reports the results of L2IR as a plug-in module for improving GNN-based fraud detection models. The experiments are conducted under more stringent conditions to evaluate the robustness of L2IR: 50% of the fraud labels are removed, and the training ratio is set to 40%. L2IR is instantiated with two base LLMs, *Qwen3-8B* and *Llama-3.1-8B*, for performance comparison.

As shown in the table, L2IR consistently improves all GNN-based methods on both datasets across the two LLM variants. With *Qwen3-8B*, L2IR brings average gains of 3.19% in AUROC and 2.57% in AUPRC on Amazon, and 2.45% and 5.54% on Yelp, respectively. With *Llama-3.1-8B*, L2IR obtains similar average gains of 3.14% and 2.37% on Amazon, and 2.34% and 5.07% on Yelp. The gains also hold for strong GNN-based methods such as RGTAN and DiffGraph. For example, L2IR improves RGTAN by 8.27% in AUPRC on Yelp and DiffGraph by 4.83% in AUPRC on Amazon. These results confirm that L2IR generalizes well to different GNN-based methods, where semantic evidence derived from behavior and connection

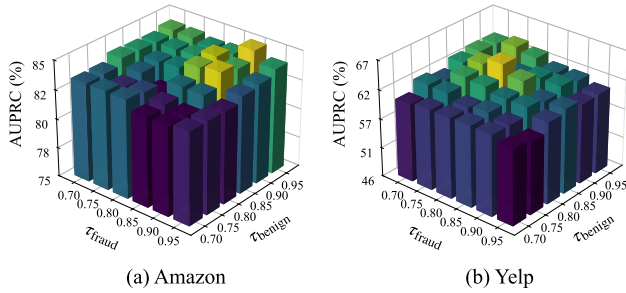


**Figure 4: Parameter sensitivity analysis on confidence thresholds  $\tau_{\text{fraud}}$  and  $\tau_{\text{benign}}$ .**

intents jointly provides reliable signals of camouflaged fraud, and the self-training mechanism effectively compensates for the insufficient labels. The consistent gains across the two LLM variants also suggest that L2IR is not sensitive to the choice of the backbone language model.

#### 5.4 Ablation Study

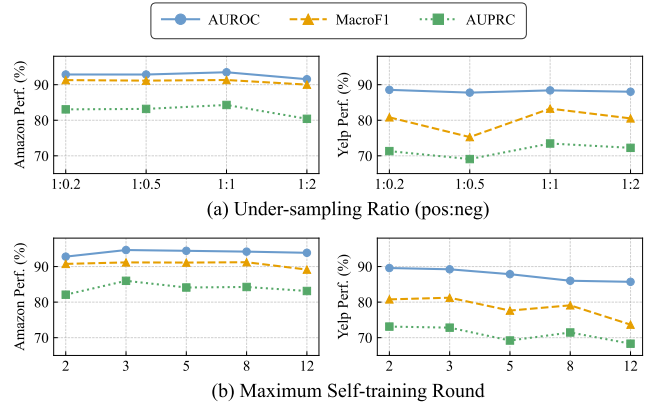
To validate the contribution of each key module in L2IR, we conduct ablation studies by integrating L2IR with five representative GNN models. Specifically, we ablate three core modules—*Behavior Intent Profiling* (BI), *Connection Intent Reasoning* (CI), and *Adaptive Self-Training* (ST). For these ablation studies, we adopt the same setting used in Table 5 where 50% of the fraud labels are removed.

Table 6 presents the ablation results of the three core components on both datasets. As shown in the table, removing any module consistently degrades performance across different GNN-based methods, confirming that these modules provide complementary benefits. Among them, CI contributes the most, as excluding it leads to the largest drop in most metrics, particularly in AUPRC. For example, AUPRC drops by 7.83%, 5.25%, and 4.50% on Yelp with BWGNN, RGTAN, and DiffGraph, respectively, confirming that *Connection Intent Reasoning* is crucial for improving detection reliability under camouflaged fraud. Removing BI also reduces performance noticeably, with AUPRC drops of 4.73% and 3.06% on Yelp with BWGNN and RGTAN, respectively, showing that semantic evidence from *Behavior Intent Profiling* helps retain fraud signals before graph aggregation. Excluding ST further decreases AUPRC by 3.21%, 2.26%, and 2.35% on Yelp with BWGNN, PMP, and RGTAN, respectively, demonstrating the effectiveness of expanding supervision with *Adaptive Self-Training*.

#### 5.5 Parameter Sensitivity Analysis

Using CARE-GNN as the backbone [4], we investigate the sensitivity of L2IR to three key parameter types on both datasets: (i) the confidence thresholds  $\tau_{\text{fraud}}$  and  $\tau_{\text{benign}}$  for adaptive self-training, (ii) the class balance ratio (positive:negative) of the training set, and (iii) the maximum number of self-training rounds.

Figure 4 presents the impact of the confidence thresholds  $\tau_{\text{fraud}}$  and  $\tau_{\text{benign}}$  on AUPRC. Amazon exhibits a broad stable region across most configurations, with peak AUPRC of 84.92% when  $\tau_{\text{benign}} = 0.95$  and  $\tau_{\text{fraud}} = 0.90$ , suggesting relatively low sensitivity to the exact threshold values. Yelp shows greater sensitivity, with



**Figure 5: Parameter sensitivity analysis on under-sampling ratio and maximum self-training round.**

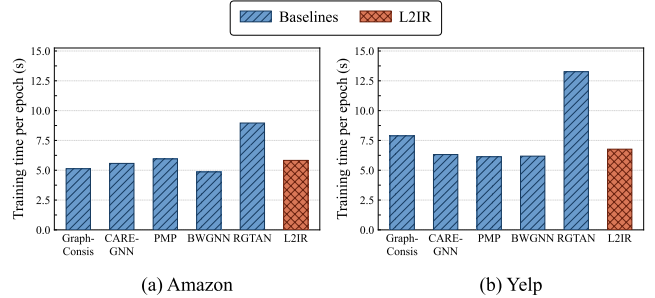


**Figure 6: Efficiency comparison on two datasets.**

AUPRC peaking at 65.03% when  $\tau_{\text{benign}} = 0.85$  and  $\tau_{\text{fraud}} = 0.80$ , and dropping when  $\tau_{\text{fraud}}$  is set too high relative to  $\tau_{\text{benign}}$ , as a looser  $\tau_{\text{benign}}$  admits more low-confidence benign pseudo-labels into training, diluting fraud signals and shifting the model toward the majority class.

Figure 5(a) evaluates the impact of varying the class balance ratio. We train L2IR under different balance ratios. Performance peaks at a 1:1 ratio on both datasets. The decline at the 1:2 ratio, particularly in MacroF1 and AUPRC, indicates that an excess of negative samples shifts the learning bias toward the benign majority. Overall, L2IR exhibits strong robustness to the class balance ratio in the training set.

Figure 5(b) illustrates the influence of maximum self-training rounds. Optimal results emerge at early stages (round 3 for Amazon and round 2 for Yelp). Extending the process to additional rounds may degrade performance, as noisy pseudo-labels can accumulate in the training set.

#### 5.6 Efficiency Analysis

We evaluate the computational efficiency of L2IR by comparing its per-epoch training time against representative baselines. As shown in Figure 6, on Amazon, L2IR achieves a per-epoch training time of 5.83s, which is comparable to CARE-GNN at 5.57s and PMP at 5.95s, while being significantly faster than RGTAN at 8.96s. On Yelp, L2IR requires 6.77s per epoch, remaining within the range of standard baselines and taking nearly half the time of RGTAN

at 13.26s, where RGTAN incurs additional cost from temporal attention and risk-aware neighborhood modeling. This efficiency of L2IR is achieved by fully decoupling the LLM inference for both behavior intent profiling and connection intent reasoning as a one-time offline preprocessing step, which bounds the online training cost to standard GNN complexity.

## 6 Conclusions

In this paper, we propose L2IR, an LLM-driven latent intent revealing framework for graph fraud detection in the presence of widespread camouflage. We design behavior intent profiling and connection intent reasoning to model the intents behind node interactions. By leveraging LLMs to infer hidden interaction intents, L2IR enhances the distinction between camouflaged fraudsters and benign entities. We also introduce adaptive self-training to improve training performance under limited fraud labels. Experiments on two real-world benchmarks show that L2IR consistently outperforms state-of-the-art baselines, particularly under low training ratios and with scarce labeled fraud. Ablation studies verify the effectiveness of the proposed designs, and importantly, these designs introduce no significant overhead compared to standard GNNs, as LLM inference is decoupled as a one-time offline preprocessing step.

## A Prompt Templates

### Prompt template for Behavior Intent Profiling

```
SYSTEM_PROMPT = """
You are a senior fraud detection analyst specializing in review behavior and relation camouflage. Your task is to infer behavior intent. Strictly follow all provided constraints and requirements.
"""

USER_PROMPT = """
You are given reference cases, target user information, graph context, neighbor distribution, and review history. The Amazon dataset contains e-commerce product reviews, where users may show fraudulent behavior through abnormal review activity and camouflaged relations.

Few-Shot Exemplars: {few-shot_exemplars}
Target User: {target_user}
Target Statistics: {target_statistics}
Graph Relation Context: {graph_relation_context}
Review Traces: {review_traces}

Task:
Analyze the target user's behavior intent. Focus on activity pattern, rating behavior, review content, helpfulness, graph context, and possible fraud signals.

Requirements:
```

```
1) **Information source**: Use only the provided information.
2) **Reference use**: Use reference cases only for comparison. Do not treat them as target labels.
3) **Context use**: Use graph relation context as supporting information. Do not infer the target label from neighbor labels alone.
4) **Balanced signals**: Consider both fraud signals and benign signals.
5) **Intent grounding**: Separate observed behavior from inferred behavior intent.
6) **Output format**: Return only four sections: User Profile Summary, Behavior Pattern Analysis, Fraud Signal Analysis, and Overall Assessment. Do not output the final class label. The output should read naturally and contain no phrasing that suggests it was produced by a language model.
"""
```

### Prompt template for Connection Intent Reasoning

```
SYSTEM_PROMPT = """
You are a senior fraud audit analyst specializing in review graphs and relation camouflage. Your task is to analyze the intent behind a suspicious connection between a suspected fraudster and a likely benign user, and assess whether this connection provides supportive or misleading evidence for fraud detection. Strictly follow all provided constraints and requirements.
"""

USER_PROMPT = """
You are given a suspicious connection, preliminary risk information, and the review histories of two connected users. The Amazon dataset contains e-commerce product reviews, where suspicious user connections may either support fraud detection or reflect relation camouflage.

Target Connection: {connection_metadata}
User A Review Traces: {user_a_reviews}
User B Review Traces: {user_b_reviews}

Task:
Analyze the connection between User A and User B. Focus on behavior difference, shared products, rating pattern, review timing, review content, helpfulness, and connection intent. Use only connection related information and do not repeat full user profiles.

Requirements:
1) **Information source**: Use only the provided information.
```

2) **\*\*Role use\*\***: Use preliminary roles and scores only as audit signals. Do not treat them as ground truth labels.

3) **\*\*Balanced judgment\*\***: Consider both supportive and misleading interpretations.

4) **\*\*Intent grounding\*\***: Separate observed behavior from inferred connection intent.

5) **\*\*Verdict format\*\***: In Risk Verdict, return the risk level as Low, Medium, or High, confidence as a number between 0 and 1, and exactly three key signals.

6) **\*\*Output format\*\***: Return only five sections: Connection Overview, Behavior Difference, Connection Intent Analysis, Counter Evidence and Uncertainty, and Risk Verdict. The output should read naturally and contain no phrasing that suggests it was produced by a language model.

""

## References

- [1] Josh Achiam, Steven Adler, Sandhini Agarwal, Lama Ahmad, Ilge Akkaya, Florencia Leoni Aleman, Diogo Almeida, Janko Altenschmidt, Sam Altman, Shyamal Anadkat, et al. 2023. Gpt-4 technical report. *arXiv preprint arXiv:2303.08774* (2023).
- [2] Leman Akoglu, Hanghang Tong, and Danai Koutra. 2015. Graph based anomaly detection and description: a survey. *Data mining and knowledge discovery* 29, 3 (2015), 626–688.
- [3] Yupeng Chang, Xu Wang, Jindong Wang, Yuan Wu, Linyi Yang, Kaijie Zhu, Hao Chen, Xiaoyuan Yi, Cunxiang Wang, Yidong Wang, et al. 2024. A survey on evaluation of large language models. *ACM transactions on intelligent systems and technology* 15, 3 (2024), 1–45.
- [4] Yingdong Dou, Zhiwei Liu, Li Sun, Yutong Deng, Hao Peng, and Philip S Yu. 2020. Enhancing graph neural network-based fraud detectors against camouflaged fraudsters. In *Proceedings of the 29th ACM international conference on information & knowledge management*. 315–324.
- [5] Aaron Grattafiori, Abhimanyu Dubey, Abhinav Jauhri, Abhinav Pandey, Abhishek Kadian, Ahmad Al-Dahle, Aiesha Letman, Akhil Mathur, Alan Schelten, Alex Vaughan, et al. 2024. The llama 3 herd of models. *arXiv preprint arXiv:2407.21783* (2024).
- [6] Will Hamilton, Zhitao Ying, and Jure Leskovec. 2017. Inductive representation learning on large graphs. *Advances in neural information processing systems* 30 (2017).
- [7] Xiaoxin He, Xavier Bresson, Thomas Laurent, Adam Perold, Yann LeCun, and Bryan Hooi. 2024. Harnessing explanations: Llm-to-llm interpreter for enhanced text-attributed graph representation learning. In *International conference on learning representations*, Vol. 2024. 5711–5732.
- [8] Bryan Hooi, Hyun Ah Song, Alex Beutel, Neil Shah, Kijung Shin, and Christos Faloutsos. 2016. FRAUDAR: Bounding Graph Fraud in the Face of Camouflage. In *Proceedings of the 22nd ACM SIGKDD international conference on knowledge discovery and data mining*. 895–904.
- [9] Tairan Huang, Yili Wang, Qitong Li, Changlong He, and Jianliang Gao. 2025. Can llms find fraudsters? multi-level llm enhanced graph fraud detection. In *Proceedings of the 33rd ACM International Conference on Multimedia*. 1530–1538.
- [10] Thomas N Kipf and Max Welling. 2016. Semi-supervised classification with graph convolutional networks. *arXiv preprint arXiv:1609.02907* (2016).
- [11] Yuan Li, Jun Hu, Bryan Hooi, Bingsheng He, and Cheng Chen. 2026. DGP: A Dual-Granularity Prompting Framework for Fraud Detection with Graph-Enhanced LLMs. In *Proceedings of the AAAI Conference on Artificial Intelligence*, Vol. 40. 15171–15179.
- [12] Zongwei Li, Lianghao Xia, Hua Hua, Shijie Zhang, Shuangyang Wang, and Chao Huang. 2025. Diffgraph: Heterogeneous graph diffusion model. In *Proceedings of the Eighteenth ACM International conference on web search and data mining*. 40–49.
- [13] Yang Liu, Xiang Ao, Zidi Qin, Jianfeng Chi, Jinghua Feng, Hao Yang, and Qing He. 2021. Pick and choose: a GNN-based imbalanced learning approach for fraud detection. In *Proceedings of the web conference 2021*. 3168–3177.
- [14] Ziqi Liu, Chaochao Chen, Longfei Li, Jun Zhou, Xiaolong Li, Le Song, and Yuan Qi. 2019. Geniepath: Graph neural networks with adaptive receptive paths. In *Proceedings of the AAAI conference on artificial intelligence*, Vol. 33. 4424–4431.
- [15] Ziqi Liu, Chaochao Chen, Xinxing Yang, Jun Zhou, Xiaolong Li, and Le Song. 2018. Heterogeneous graph neural networks for malicious account detection. In *Proceedings of the 27th ACM international conference on information and knowledge management*. 2077–2085.
- [16] Zhiwei Liu, Yingdong Dou, Philip S Yu, Yutong Deng, and Hao Peng. 2020. Alluviating the inconsistency problem of applying graph neural network to fraud detection. In *Proceedings of the 43rd international ACM SIGIR conference on research and development in information retrieval*. 1569–1572.
- [17] Mingxuan Lu, Zhichao Han, Susie Xi Rao, Zitao Zhang, Yang Zhao, Yanan Shan, Ramesh Raghunathan, Ce Zhang, and Jiawei Jiang. 2022. Bright-graph neural networks in real-time fraud detection. In *Proceedings of the 31st ACM international conference on information & knowledge management*. 3342–3351.
- [18] Julian John McAuley and Jure Leskovec. 2013. From amateurs to connoisseurs: modeling the evolution of user expertise through online reviews. In *Proceedings of the 22nd international conference on World Wide Web*. 897–908.
- [19] Shervin Minaee, Tomas Mikolov, Narjes Nikzad, Meysam Chenaghlu, Richard Socher, Xavier Amatriain, and Jianfeng Gao. 2024. Large language models: A survey. *arXiv preprint arXiv:2402.06196* (2024).
- [20] Shebuti Rayana and Leman Akoglu. 2015. Collective opinion spam detection: Bridging review networks and metadata. In *Proceedings of the 21th ACM SIGKDD international conference on knowledge discovery and data mining*. 985–994.
- [21] Fengzhao Shi, Yanan Cao, Yanmin Shang, Yuchen Zhou, Chuan Zhou, and Jia Wu. 2022. H2-fdetector: A gnn-based fraud detector with homophilic and heterophilic connections. In *Proceedings of the ACM web conference 2022*. 1486–1494.
- [22] Yanchao Tan, Zihao Zhou, Hang Lv, Weiming Liu, and Carl Yang. 2023. Walkm: A uniform language model fine-tuning framework for attributed graph embedding. *Advances in neural information processing systems* 36 (2023), 13308–13325.
- [23] Jianheng Tang, Jiajin Li, Ziqi Gao, and Jia Li. 2022. Rethinking graph neural networks for anomaly detection. In *International conference on machine learning*. PMLR, 21076–21089.
- [24] Jiabin Tang, Yuhao Yang, Wei Wei, Lei Shi, Lixin Su, Suqi Cheng, Dawei Yin, and Chao Huang. 2024. Graphgpt: Graph instruction tuning for large language models. In *Proceedings of the 47th International ACM SIGIR Conference on Research and Development in Information Retrieval*. 491–500.
- [25] Arun James Thirunavukarasu, Darren Shu Jeng Ting, Kabilan Elangovan, Laura Gutierrez, Ting Fang Tan, and Daniel Shu Wei Ting. 2023. Large language models in medicine. *Nature medicine* 29, 8 (2023), 1930–1940.
- [26] Petar Veličković, Guillem Cucurull, Arantxa Casanova, Adriana Romero, Pietro Lio, Yoshua Bengio, et al. 2018. Graph attention networks. In *International conference on learning representations*, Vol. 6. Ithaca.
- [27] Petar Veličković, William Fedus, William L Hamilton, Pietro Liò, Yoshua Bengio, and R Devon Hjelm. 2018. Deep graph infomax. *arXiv preprint arXiv:1809.10341* (2018).
- [28] Daixin Wang, Jianbin Lin, Peng Cui, Quanhui Jia, Zhen Wang, Yanming Fang, Quan Yu, Jun Zhou, Shuang Yang, and Yuan Qi. 2019. A semi-supervised graph attentive network for financial fraud detection. In *2019 IEEE international conference on data mining (ICDM)*. IEEE, 598–607.
- [29] Jianyu Wang, Rui Wen, Chunming Wu, Yu Huang, and Jian Xiong. 2019. Fdgars: Fraudster detection via graph convolutional networks in online app review system. In *Companion proceedings of the 2019 World Wide Web conference*. 310–316.
- [30] Xiao Wang, Meiqi Zhu, Deyu Bo, Peng Cui, Chuan Shi, and Jian Pei. 2020. Amgen: Adaptive multi-channel graph convolutional networks. In *Proceedings of the 26th ACM SIGKDD International conference on knowledge discovery & data mining*. 1243–1253.
- [31] Wei Wei, Xubin Ren, Jiabin Tang, Qinyong Wang, Lixin Su, Suqi Cheng, Junfeng Wang, Dawei Yin, and Chao Huang. 2024. Llmrec: Large language models with graph augmentation for recommendation. In *Proceedings of the 17th ACM international conference on web search and data mining*. 806–815.
- [32] Haiqin Weng, Shouling Ji, Fuzheng Duan, Zhao Li, Jianhai Chen, Qinning He, and Ting Wang. 2019. Cats: cross-platform e-commerce fraud detection. In *2019 IEEE 35th international conference on data engineering (icde)*. IEEE, 1874–1885.
- [33] Sheng Xiang, Guibin Zhang, Dawei Cheng, and Ying Zhang. 2025. Enhancing attribute-driven fraud detection with risk-aware graph representation. *IEEE Transactions on Knowledge and Data Engineering* (2025).
- [34] An Yang, Anfeng Li, Baosong Yang, Beichen Zhang, Binyuan Hui, Bo Zheng, Bowen Yu, Chang Gao, Chengen Huang, Chenxu Lv, et al. 2025. Qwen3 technical report. *arXiv preprint arXiv:2505.09388* (2025).
- [35] Chengdong Yang, Hongrui Liu, Daixin Wang, Zhiqiang Zhang, Cheng Yang, and Chuan Shi. 2025. Flag: Fraud detection with llm-enhanced graph neural network. In *Proceedings of the 31st ACM SIGKDD Conference on Knowledge Discovery and Data Mining V. 2*. 5150–5160.
- [36] Ruosong Ye, Caiqi Zhang, Runhui Wang, Shuyuan Xu, and Yongfeng Zhang. 2024. Language is all a graph needs. In *Findings of the association for computational linguistics: EACL 2024*. 1955–1973.
- [37] Hang Yu, Zhengyang Liu, and Xiangfeng Luo. 2024. Barely supervised learning for graph-based fraud detection. In *Proceedings of the AAAI conference on artificial intelligence*, Vol. 38. 16548–16557.

- [38] Yiming Zhang, Yujie Fan, Yanfang Ye, Liang Zhao, and Chuan Shi. 2019. Key player identification in underground forums over attributed heterogeneous information network embedding framework. In *Proceedings of the 28th ACM international conference on information and knowledge management*. 549–558.
- [39] Jianan Zhao, Meng Qu, Chaozhuo Li, Hao Yan, Qian Liu, Rui Li, Xing Xie, and Jian Tang. 2022. Learning on large-scale text-attributed graphs via variational inference. *arXiv preprint arXiv:2210.14709* (2022).
- [40] Jing Zhu, Xiang Song, Vassilis Ioannidis, Danai Koutra, and Christos Faloutsos. 2024. Touchup-g: Improving feature representation through graph-centric fine-tuning. In *Proceedings of the 47th International ACM SIGIR Conference on Research and Development in Information Retrieval*. 2662–2666.
- [41] Yanqiao Zhu, Yichen Xu, Feng Yu, Qiang Liu, Shu Wu, and Liang Wang. 2020. Deep graph contrastive representation learning. *arXiv preprint arXiv:2006.04131* (2020).
- [42] Wei Zhuo, Zemin Liu, Bryan Hooi, Bingsheng He, Guang Tan, Rizal Fathony, and Jia Chen. 2024. Partitioning message passing for graph fraud detection. *arXiv preprint arXiv:2412.00020* (2024).